A 10–15-Yr Modulation Cycle of ENSO Intensity

FENGPENG SUN* AND JIN-YI YU

Department of Earth System Science, University of California, Irvine, Irvine, California

ABSTRACT

This study examines the slow modulation of El Niño–Southern Oscillation (ENSO) intensity and its underlying mechanism. A 10–15-yr ENSO intensity modulation cycle is identified from historical and paleoclimate data by calculating the envelope function of boreal winter Niño-3.4 and Niño-3 sea surface temperature (SST) indices. Composite analyses reveal interesting spatial asymmetries between El Niño and La Niña events within the modulation cycle. In the enhanced intensity periods of the cycle, El Niño is located in the eastern tropical Pacific and La Niña in the central tropical Pacific. The asymmetry is reversed in the weakened intensity periods: El Niño centers in the central Pacific and La Niña in the eastern Pacific. El Niño and La Niña centered in the eastern Pacific are accompanied with basin-scale surface wind and thermocline anomalies, whereas those centered in the central Pacific are accompanied with local wind and thermocline anomalies. The El Niño–La Niña asymmetries provide a possible mechanism for ENSO to exert a nonzero residual effect that could lead to slow changes in the Pacific mean state. The mean state changes are characterized by an SST dipole pattern between the eastern and central tropical Pacific, which appears as one leading EOF mode of tropical Pacific decadal variability. The Pacific Walker circulation migrates zonally in association with this decadal mode and also changes the mean surface wind and thermocline patterns along the equator. Although the causality has not been established, it is speculated that the mean state changes in turn favor the alternative spatial patterns of El Niño and La Niña that manifest as the reversed ENSO asymmetries. Using these findings, an ENSO–Pacific climate interaction mechanism is hypothesized to explain the decadal ENSO intensity modulation cycle.

1. Introduction

El Niño–Southern Oscillation (ENSO) is known to undergo decadal (and interdecadal) variations in its frequency, intensity, and propagation pattern (e.g., Wang and Wang 1996; An and Wang 2000; Fedorov and Philander 2000; Timmermann 2003; An and Jin 2004; Yeh and Kirtman 2004). The decadal ENSO variability and its potential influences on global climate and weather have prompted extensive research (e.g., Torrence and Webster 1999; Power et al. 1999). Various hypotheses have been put forward to explain the origin of decadal ENSO variability. Initially, the decadal ENSO variability was suggested to be forced by extratropical processes (e.g., Barnett et al. 1999; Pierce et al. 2000) or arise from tropical–extratropical interactions (e.g., Gu and Philander 1997; Wang and Weisberg 1998; Zhang et al. 1998). More recent studies have suggested the decadal ENSO variability could originate internally within the tropics and does not require the involvement of extratropical processes (e.g., Knutson et al. 1997; Kirtman and Schopf 1998; Timmermann and Jin 2002; Timmermann 2003). The decadal ENSO variability was described as either an internal mode of the coupled atmosphere–ocean system in the tropics (e.g., Knutson et al. 1997; Kirtman and Schopf 1998; Timmermann and Jin 2002) or excited by stochastic forcing (e.g., Penland and Sardeshmukh 1995; Eckert and Latif 1997; Newman et al. 2003). Demonstrated with a simple model, Newman et al. (2003) and Newman (2007) further suggested that the decadal variability in the extratropics, such as the Pacific decadal oscillation (PDO; Mantua et al. 1997), could be forced by the decadal ENSO variability via an

---

* Current affiliation: Department of Atmospheric and Oceanic Sciences, University of California, Los Angeles, Los Angeles, California.

Corresponding author address: Dr. Jin-Yi Yu, Department of Earth System Science, University of California, Irvine, Irvine, CA 92697-3100.
E-mail: jyyu@uci.edu

"atmospheric bridge" (Alexander et al. 2002). The observational study of Deser et al. (2004) also suggested that the tropical Pacific plays a key role in North Pacific interdecadal climate variability.

For the tropical-origin hypothesis, slow changes in the tropical Pacific mean state have been considered to account for the decadal ENSO variability. Modeling studies showed that the ENSO amplitude is sensitive to the mean thermocline depth (Zebiak and Cane 1987; Latif et al. 1993), mean zonal SST gradient (Knutson et al. 1997), and mean vertical structure of the upper ocean (Meehl et al. 2001). The recurrence frequency and growth rates of ENSO were shown to depend on these mean state properties in the equatorial Pacific (Fedorov and Philander 2000). Modeling studies (e.g., Kirtman and Schopf 1998) also showed ENSO dynamics could alternate between the delayed-oscillator (Suarez and Schopf 1988; Battisti and Hirst 1989) type and the stochastically forced type as the Pacific state changes, and it leads to decadal variability in ENSO properties. More recently, the nonlinear ENSO dynamics and the interactions between ENSO and the Pacific mean state have been increasingly emphasized to explain the decadal ENSO variability. Timmermann and Jin (2002) used a low-order tropical atmosphere–ocean model to show that changing the strength of zonal SST advection can alternate ENSO periods between biennial and 4–5 yr and result in a slow amplitude modulation. By analyzing long-term coupled general circulation model (CGCM) simulations, Timmermann (2003) further suggested decadal ENSO modulation could also result from the nonlinear interactions between ENSO and the Pacific background state. Rodgers et al. (2004) and An and Jin (2004) pointed out that ENSO has strong nonlinearity that can cause asymmetries between its warm (El Niño) and cold (La Niña) phases. Rodgers et al. (2004) analyzed the long-term integration of the ECHO-G model and found the decadal ENSO variability contributes to the structure of the tropical Pacific decadal variability in the model, resulting from the asymmetry between the model's El Niño and La Niña. Sun and Zhang (2006) conducted numerical experiments with and without ENSO using a coupled model to show that ENSO works as a basin-scale mixer to regulate the time-mean thermal stratification in the upper-equatorial Pacific. These latest studies pointed out that further studies of the ENSO–Pacific climate interaction are important and needed to better understand the affect of ENSO variability on decadal time scales.

It was noticed that extreme ENSO events occur approximately every 10–20 yr (e.g., Gu and Philander 1995; Torrence and Webster 1999), recalling that the last three strongest ENSO events occurred in 1972/73,

1982/83, and 1997/98. Between those strong events, rather weaker ENSO events happened. Does this nearly 10–20-yr time scale happen by chance or is there a decadal modulation cycle of ENSO intensity? What is the possible underlying mechanism? To address these questions, we analyzed various atmospheric and oceanic datasets for the existence of slow modulations of ENSO intensity and to describe the changes of ENSO and tropical Pacific mean state during the modulation. The datasets and the analysis methods are outlined in section 2, followed by the identification of an ENSO modulation cycle in section 3. In section 4, the asymmetric spatial structures of ENSO within the modulation cycle are described. In section 5, a linkage is established between the ENSO asymmetries and one leading mode of the decadal mean state changes in the tropical Pacific. Major findings are summarized in section 6. An ENSO asymmetry-mean state interaction mechanism is also hypothesized to explain the observed decadal ENSO modulation cycle.

2. Datasets and methods

Two historical SST datasets are used in this study: 1) the global monthly Extended Reconstructed Sea Surface Temperature dataset version 2 (ERSST.v2; Smith and Reynolds 2004) with a spatial resolution of $2° \times 2°$ and 2) the Hadley Centre Sea Ice and Sea Surface Temperature dataset version 1 (HadISST1; Rayner et al. 2003) with a spatial resolution of $1° \times 1°$. The large-scale variations in HadISST1 are broadly consistent with those in ERSST.v2, but there are differences between these two datasets due to different historical bias corrections as well as different data and analysis procedures (Smith and Reynolds 2003). Most of the analyses presented in this paper are based on ERSST.v2, and HadISST1 is used for verification. ERSST.v2 is an improved extended reconstruction of the previous version, ERSST (Smith and Reynolds 2003), which is constructed using the most recently available International Comprehensive Ocean–Atmosphere Data Set (ICOADS) SST data and the improved statistical methods that allow stable reconstruction using sparse data. The analyzed signal in the historical datasets is heavily damped before 1880, so data from 1880 to 2006 is analyzed in this study. A 331-yr (1650–1980) ENSO index time series reconstructed by Mann et al. (2000) from multiproxy paleoclimate data is also used to further verify the decadal signals identified from the historical datasets. The reconstructed index represents the extended boreal winter (October–March) SST anomalies averaged in the Niño-3 region (5°S–5°N, 150°–90°W) with the long-term climatology removed.
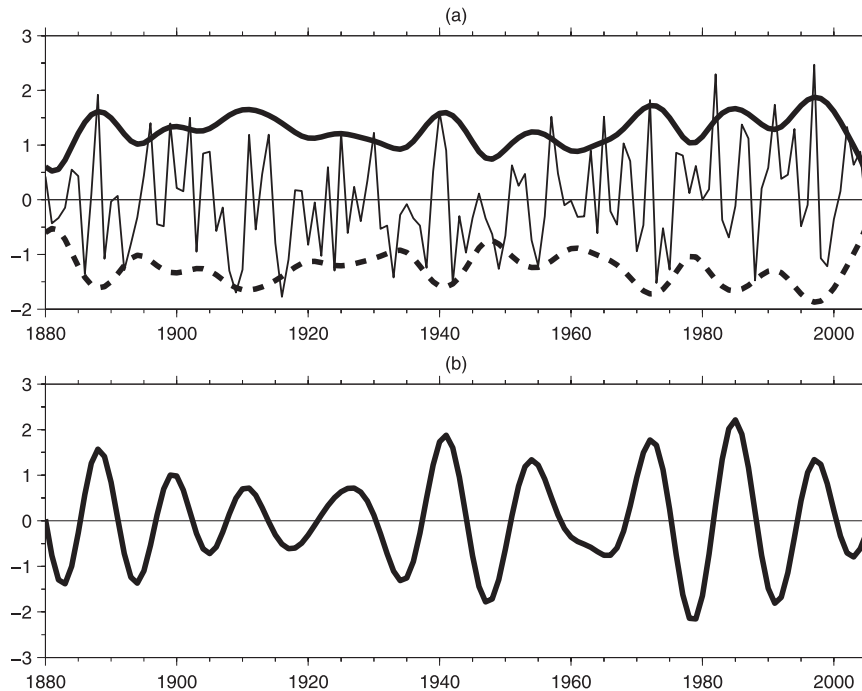
FIG. 1. (a) Time series of extended boreal winter (October–March) Niño-3.4 SST anomaly index (thin line), decadal amplitude (square root of ENVF; thick solid line), and its mirror (thick dashed line). (b): Standardized 10–20-yr bandpass-filtered ENVF.

Also used in this study are the monthly surface wind and 200-hPa velocity potential data from the National Centers for Environmental Prediction (NCEP)–National Center for Atmospheric Research (NCAR) reanalysis data (Kalnay et al. 1996) and the monthly upper-ocean temperature data from Simple Ocean Data Assimilation (SODA; Carton et al. 2000). The surface wind data is on 2.5° × 2.5° grids, the velocity potential data is on the Gaussian grids (1.875° × ~2°), and both datasets are from 1948 to 2005. SODA assimilates the ocean observations, for example, World Ocean Atlas, XBT profiles, in situ station data, and satellite altimeter–derived sea level data. The upper-ocean temperature data from SODA has a horizontal resolution of 1° × 0.5°~1° (enhanced resolution in tropics), 15 m vertical from the surface, about 160 m deep (with lower resolution below) and is from 1950 to 2001. The temperatures are linearly interpolated in the vertical to locate the depth of 20°C isotherms, which is used as a proxy for thermocline depth. The yearly ocean heat content (OHC; defined as the averaged temperature between surface and 300 m deep) dataset from Levitus et al. (2005) for the period of 1955–2003 is also used. Monthly anomalies for all the variables are constructed as the deviations from their monthly-mean climatologies calculated from the entire data period.

Because of ENSO's phase locking to the seasonal cycle, the mature phases of El Niño and La Niña tend to occur toward the end of the calendar year (Rasmusson and Carpenter 1982). In this study, we choose the extended boreal winter (October–March) SST anomalies in the Niño-3.4 region (5°S–5°N, 170°–120°W) to describe the variations of ENSO activity. Both Niño-3.4 and Niño-3 (used in the proxy paleoclimate dataset) regions are located within the areas where large ENSO SST variability occurs, and their time evolutions are highly correlated.

3. The 10–15-yr modulation cycle of ENSO intensity

Figure 1a shows the extended winter Niño-3.4 index (thin solid line) calculated from the ERSST.v2. The time series has been high-pass filtered with an 8-yr cutoff to highlight the SST fluctuations on interannual ENSO time scales, considering ENSO is known to have a periodicity of 2–8 yr. The filter we used is the fourth order Butterworth filter (Parks and Burrus 1987), which is a recursive filter commonly used in climate analysis. Besides the dominant interannual ENSO events, also seen in the time series is a modulation of ENSO intensity—periods of strong and weak ENSO intensity alternate on slow time scales. We used an "envelope function" (ENVF) adopted from Nakamura and Wallace (1990) to quantify the modulation of ENSO intensity. To construct the envelope

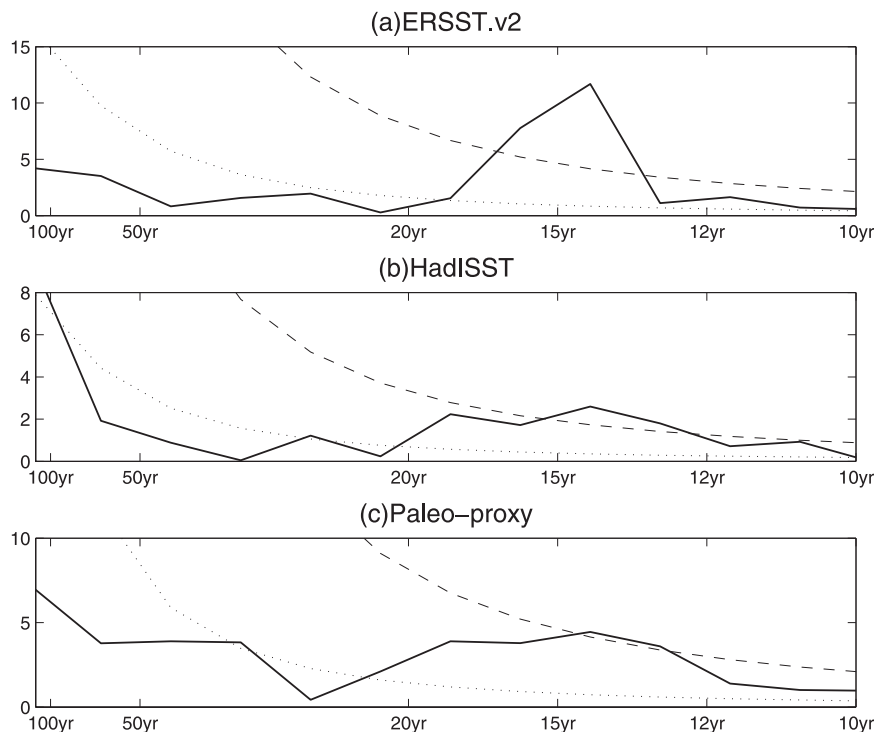## (a)ERSST.v2

(b)HadISST

(c)Paleo–proxy

FIG. 2. Power spectrum of standardized ENVF of extended winter Niño-3.4 index for (a) ERSST.v2, (b) HadISST1, and (c) extended winter Niño-3 index reconstructed from the paleoclimate proxy data of Mann et al. (2000). The low-pass filtering procedure–induced serial dependence and effect on the "effective sample size" and the degrees of freedom are considered. Dotted line is the best-fit AR1 red noise power spectrum and dashed line is the 95% significance level (SL) using f test.

function, the Niño-3.4 index was first squared and then filtered with a 10-yr cut-off low-pass Butterworth filter to highlight the decadal signals. The resulting quantity was multiplied by two in recognition of the fact that the "power" of a pure harmonic oscillation of arbitrary frequency averaged over one certain period is just half the squared intensity of the oscillation (Nakamura and Wallace 1990). The resulting series is defined as the ENVF of the Niño-3.4 index. The square root of this time series represents the "true" amplitude of the slow (>10 yr) modulation. It is shown in Fig. 1a that the square-rooted ENVF (thick solid line with thick dashed line as the mirror image) portrays the slow-intensity variations of the Niño-3.4 index reasonably well. The ENVF is not sensitive to the low-pass cut-off frequency used. We also tried low-pass filters with 8- and 12-yr cutoffs and obtained a similar ENVF time series.

The power spectrum of the standardized ENVF is shown in Fig. 2a, together with the best-fit first-order autoregression (AR1) red noise spectrum and associated 95% confidence limit using an f test. The serial dependence in the time series induced by the low-pass filtering procedure and its effects on the "effective sample size" and the degree of freedom have been taken into account (Wilks 1995). It shows that the ENVF has a statistically significant spectral peak around the 10–15-yr bands. To verify this spectral peak, we also calculated the ENVFs for the Niño-3.4 index of HadISST1 and the 331-yr reconstructed Niño-3 index of Mann et al. (2000). Both indices were calculated in the extended boreal winter. Figures 2b and 2c show the power spectra of the standardized ENVFs from these two datasets. Similar to Fig. 2a, spectral peaks near the 10–15-yr bands are also evident and statistically significant at the 95% confidence level. All the three datasets consistently indicate that ENSO intensity undergoes decadal modulations, with a significantly distinct 10–15-yr cycle. To further verify the 10–15-yr modulation cycle exists in ENSO intensity, the same analysis procedure was applied to the Southern Oscillation index (SOI), the atmospheric component of ENSO. The Troup SOI dataset (Troup 1965), which is the standardized anomaly of the mean sea level pressure difference between Tahiti (17.6°S, 149.6°W) and Darwin (12.4°S, 130.9°E) from 1870 to 2006, is used.

A significant spectral peak near the 10–15-yr period was also found (not shown).

It is noted from Fig. 1a that the Niño-3.4 intensity increases toward both ends of the time series compared with the middle period of 1920–60. This indicates a secular change of ENSO variance (Gu and Philander 1995) that is far longer than the 10–15-yr decadal modulation cycle in which we are interested. For this reason, a bandpass Butterworth filter with cutoffs at 10 and 20 yr is applied to the ENVF to retain only the decadal (10–20 yr) ENSO modulation. The standardized bandpass filtered ENVF calculated from ERSST.v2 is shown in Fig. 1b. This bandpass-filtered ENVF is used as the reference time series for composite analyses in the rest of the study. We also calculated the corresponding bandpass-filtered ENVF from the HadISST1 Niño-3.4 index (not shown) and found it largely coincides with that shown in Fig. 1b, except for the periods around 1910–20 and 1930–40. The differences in these two periods may be due to the paucity of the observational data during the two world wars and to different historical bias correction methods used in those two datasets. It is worth noting that the bandpass-filtered ENVF of the SOI (not shown) is generally very consistent with the one shown in Fig. 1b.

4. Variations of ENSO structures in the modulation cycle

We examine in this section the variations of the El Niño and La Niña spatial structures within the 10–15-yr ENSO intensity modulation cycle. The anomalous surface and subsurface structures of El Niño and La Niña were composed for the enhanced and weakened intensity periods of the modulation cycle. Here, we define the enhanced and weakened intensity periods as the times when the bandpass-filtered ENVF (Fig. 1b) is greater and less than 0.3 standard deviations, respectively. These criteria were subjectively selected to have enough events for the composite. El Niño and La Niña events are defined as the events whose extended boreal winter Niño-3.4 index is greater than 0.5°C and less than −0.5°C, respectively. It should be noted that our results are not very sensitive to the thresholds used to define the El Niño/La Niña events or the enhanced/weakened intensity periods.

The composite ENSO SST anomaly structures calculated from unfiltered ERSST.v2 are shown in Figs. 3a–d, with the shading indicating 95% significant level using a t test. There are two major features in the composites. The first major feature is the evident spatial asymmetries

between El Niño and La Niña events in both the enhanced and weakened intensity periods of the modulation cycle. The second major feature is that the spatial asymmetries in the enhanced and weakened intensity periods are reversed. During the enhanced intensity periods, El Niño events (Fig. 3a) have their largest positive SST anomalies in the eastern tropical Pacific (centered at 130°W), whereas La Niña events (Fig. 3b) have their largest negative SST anomalies in the central tropical Pacific (centered at 150°W). SST anomalies of El Niño events are attached to the South America coast, whereas those of La Niña events are detached from the coast. During the weakened intensity periods, the spatial asymmetry between El Niño and La Niña still exists but is reversed from that in the enhanced intensity periods: El Niño events (Fig. 3c) are now more detached from the South America coast with significant positive SST anomalies centered in the central Pacific (near 160°W), whereas La Niña events (Fig. 3d) have significant negative SST anomalies centered in the far eastern Pacific (near 110°W) and are more attached to the coast. Kao and Yu (2009) referred to the ENSO events with their SST anomaly center in the eastern Pacific as the eastern Pacific type of ENSO and those with their SST anomaly center in the central Pacific as the central Pacific type of ENSO.

The same composite analyses were repeated with HadISST1, and similar results are found in Figs. 3e–h. The El Niño composite calculated from HadISST1 during the enhanced intensity periods (Fig. 3e) has its largest positive SST anomalies (centered at 100°W) more attached to the coast than those calculated from ERSST.v2 (Fig. 3a). Both datasets show that the El Niño–La Niña spatial asymmetries are characterized by alternations of ENSO SST anomaly centers between the central and eastern tropical Pacific. To address the concern of general paucity of data prior to 1950s for both ERSST.v2 and HadISST1, we repeated the composite analyses with only the data before and after 1950, and qualitatively similar results were found for both datasets (not shown).

The composites in Fig. 3 suggest the 10–15-yr ENSO intensity modulation cycle is accompanied by the alternation of SST anomaly centers between the eastern and central tropical Pacific for both El Niño and La Niña events. We are not aware that such reversed asymmetries have even been shown for decadal ENSO variability in observations. Timmermann (2003) remarked similar reversed asymmetries and zonal displacement of ENSO in the decadal modulation of the ENSO events produced from the ECHAM4/Ocean Isopycnal Model (OPYC3) CGCM. However, he did not show how the reversed asymmetries look like in
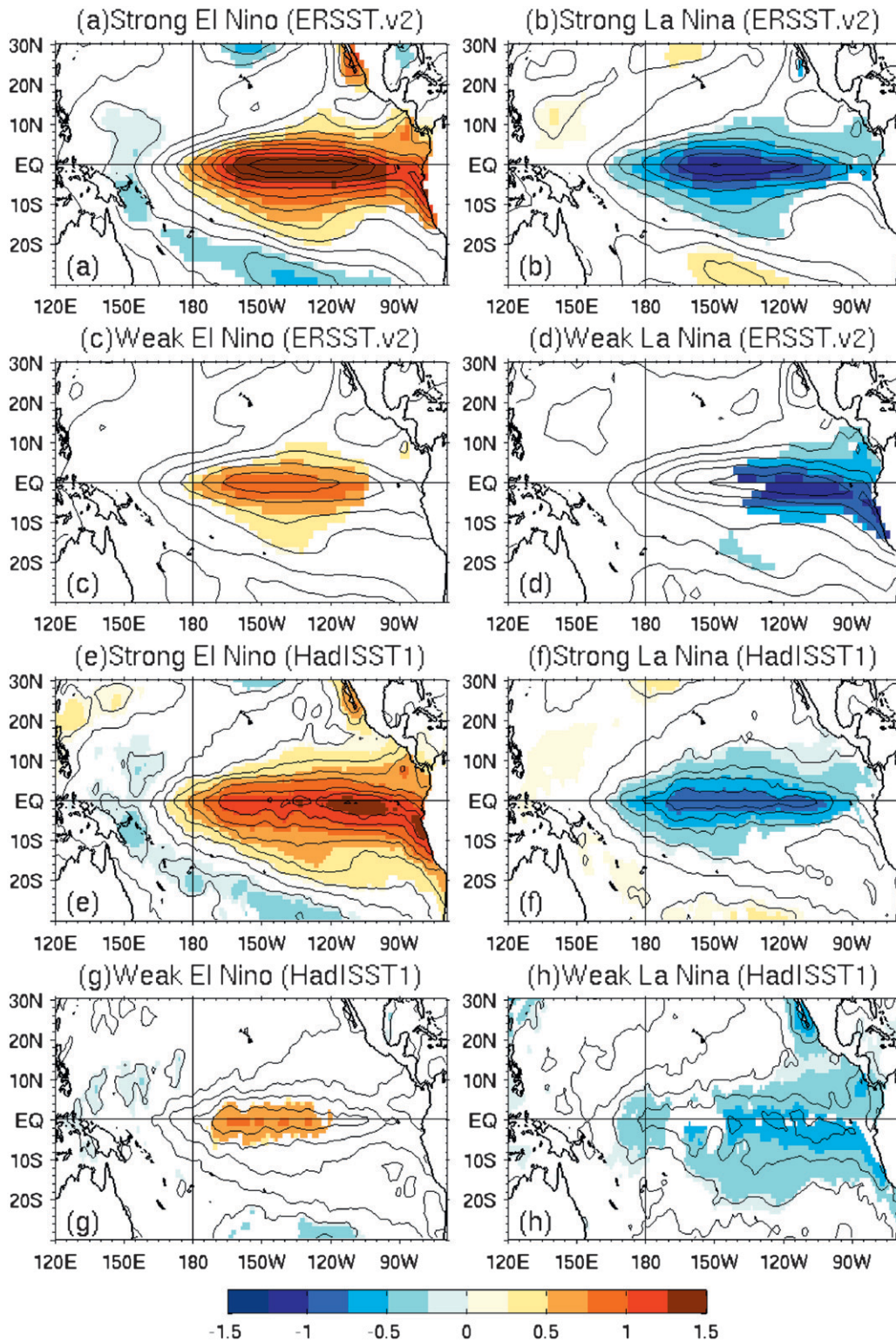
FIG. 3. Composite extended winter SST anomalies (ERSST.v2) for (a) El Niño and (b) La Niña events for the enhanced ENSO intensity periods. (c),(d) Same as (a) and (b) but for the weakened ENSO intensity periods. Contour interval (CI) is 0.2°C, and shading indicates 95% SL using a *t* test. (e)–(h) As in (a)–(d), but for HadISST1.
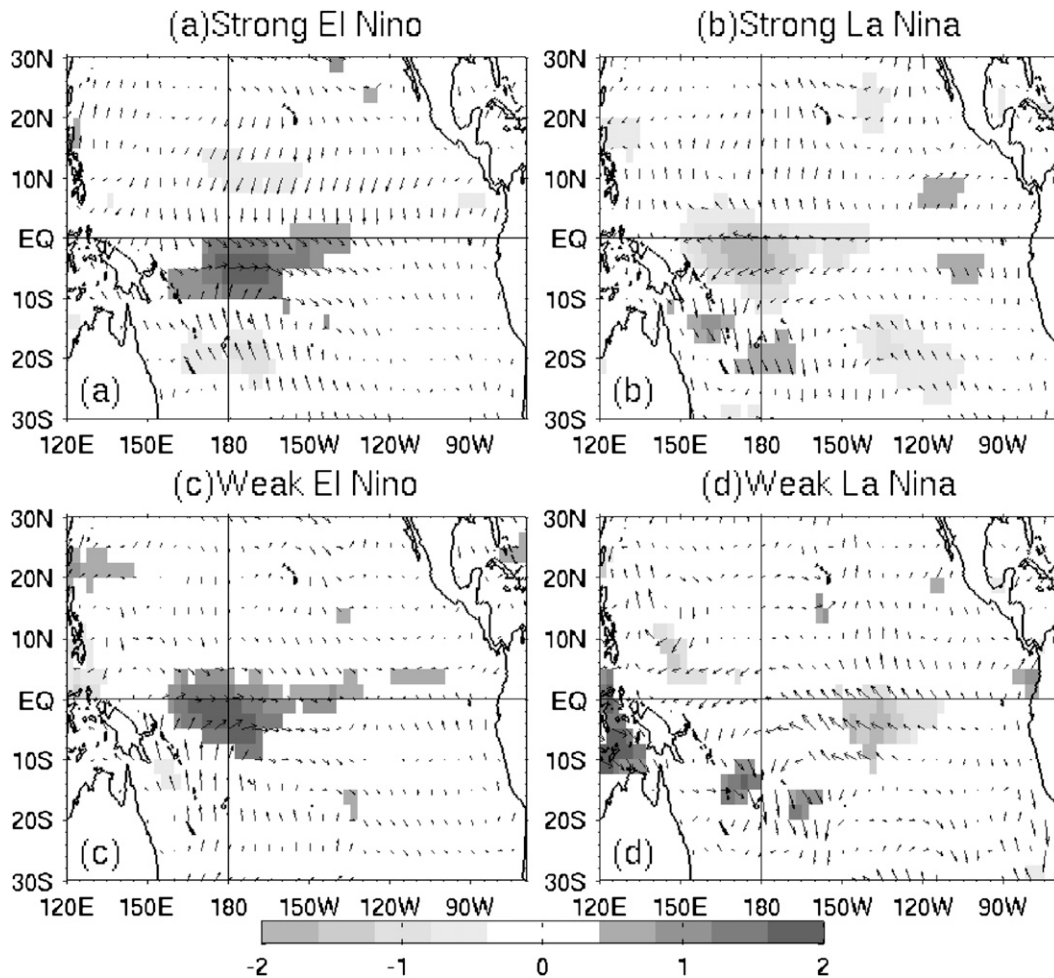
FIG. 4. Composite extended winter surface zonal wind (shading; m s^{-1}) and wind vector anomalies for (a) El Niño and (b) La Niña events for the enhanced ENSO intensity periods. (c), (d) As in (a) and (b), but for the weakened ENSO intensity periods. Shading indicates the 95% SL using a t test.

the model, so it cannot be determined how similar or different the reversed asymmetries in CGCM are to the observed asymmetries reported here.

We further show in Fig. 4 the composites of anomalous surface wind for the El Niño and La Niña events during the enhanced and weakened intensity periods. Fifty-seven years (1948–2005) of NCEP–NCAR reanalysis wind data were used. Also shown in the figure are the zonal wind anomalies (shaded) that are statistically significant at the 95% significant level using a t test. For the ENSO events with SST anomaly centers located in the eastern Pacific (i.e., the strong El Niño event in Fig. 4a and the weak La Niña event in Fig. 4d), they tend to be associated with significant anomalous surface wind vectors across the Pacific basin with the largest zonal wind anomalies located mostly to the east of the date line. For the ENSO events with SST anomaly centers located in the central Pacific (i.e., the

weak El Niño event in Fig. 4c and the strong La Niña event in Fig. 4b), their associated anomalous surface wind vectors are confined more locally in the central Pacific and their largest zonal wind anomalies are located more to the west of the date line. The anomalous wind patterns are consistent with the anomalous SST patterns. Figure 4 suggests that the eastern Pacific type of ENSO appears to involve air–sea interactions over a large portion of the tropical Pacific basin, and the central Pacific type of ENSO appears to involve air–sea interactions that are more confined in the central tropical Pacific.

The composite OHC anomalies for these strong and weak El Niño and La Niña events are show in Fig. 5. Anomalies at the 95% significance level are shaded. Here, the OHC is defined as the ocean temperature averaged over the upper 300 m, and the 1955–2003 yearly OHC values from the Levitus dataset (Levitus
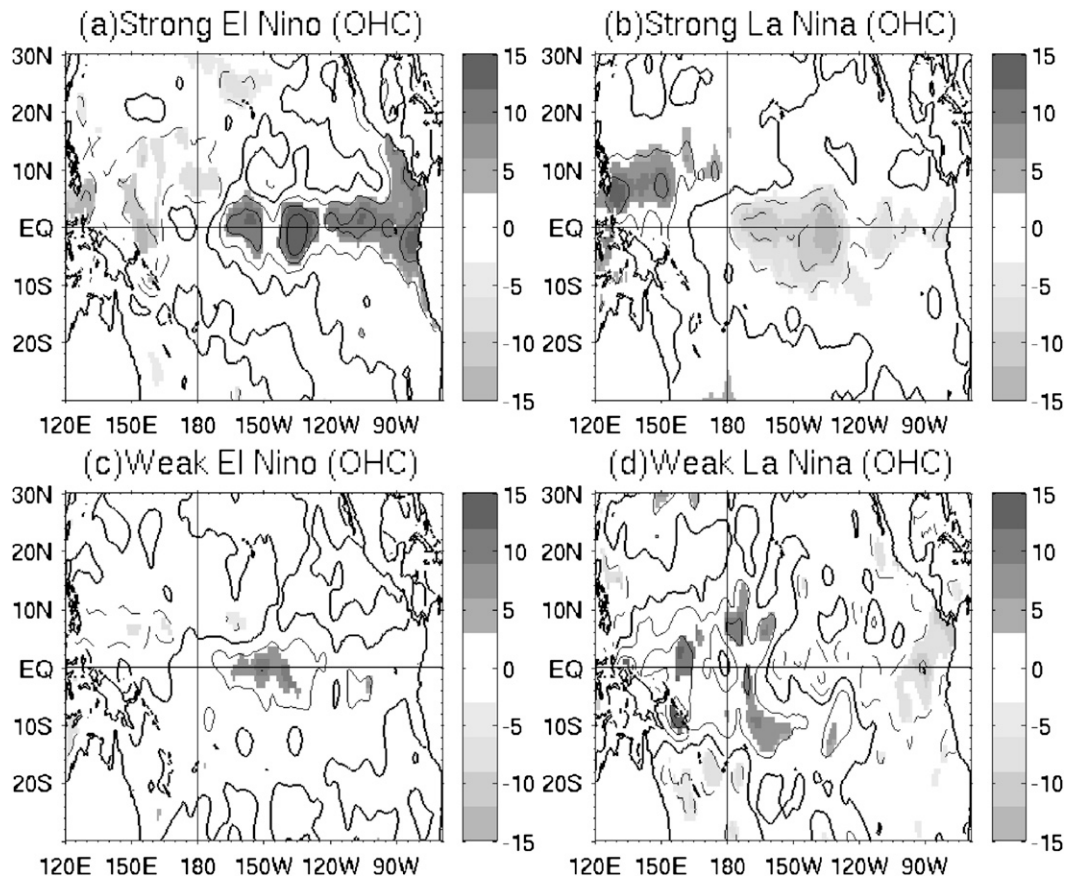
FIG. 5. Composite extended winter ocean heat content anomalies (10^{18} joules) for (a) El Niño and (b) La Niña events for the enhanced ENSO intensity periods. (c),(d) As in (a) and (b), but for the weakened ENSO intensity periods. CI is 5×10^{18}, and shading indicates the 95% SL using a t test. The zero contour line is highlighted.

et al. 2005) are used. Both strong El Niño (Fig. 5a) and weak La Niña (Fig. 5d) composites are associated with large OHC anomalies on both sides of the tropical Pacific basin. For the strong El Niño (Fig. 5a), the positive OHC anomalies extending from 170°W to the South America coast indicate a deepening thermocline along the equator. For the weak La Niña (Fig. 5d), the negative OHC anomalies in the far eastern Pacific from 120° to 90°W indicate a shoaling thermocline. The out-of-phase relationship between the anomalies in the eastern and western Pacific indicates a basin-wide thermocline variation. It is consistent with the larger zonal extents of surface wind anomaly patterns shown in Fig. 4a and Fig. 4d for these eastern Pacific types of ENSO. For the strong La Niña (Fig. 5b) and weak El Niño (Fig. 5c) composites, their associated OHC anomalies are confined mostly in the central Pacific, spanning from 180° to 130°W for strong La Niña and from 170° to 140°W for weak El Niño. These local OHC anomaly patterns also are consistent with the more confined wind anomaly patterns shown

in Figs. 4b and 4c for these central Pacific types of ENSO.

The spatial asymmetry between strong El Niño and La Niña events has been noticed for some time (e.g., Hoerling et al. 1997; Monahan 2001), and it was explained as a result of nonlinearity, such as horizontal and vertical advection in ENSO dynamics (e.g., An and Jin 2004; Dong 2005; Schopf and Burgman 2006). Our results show the spatial asymmetry also exists between weak El Niño and weak La Niña, suggesting that explanations other than the ENSO nonlinearity may be needed. One possibility is that the ENSO asymmetries may reflect different types of ENSO dynamics. For example, the two patterns of ENSO events (i.e., the one centered in the eastern Pacific and the other centered in the central Pacific) might be the exhibitions of two ENSO types, such as the delayed oscillator mode (Suarez and Schopf 1988; Battisti and Hirst 1989) and the slow SST mode (Neelin 1991; Neelin and Jin 1993; Jin and Neelin 1993a,b), or others. Further examinations of this possibility are important
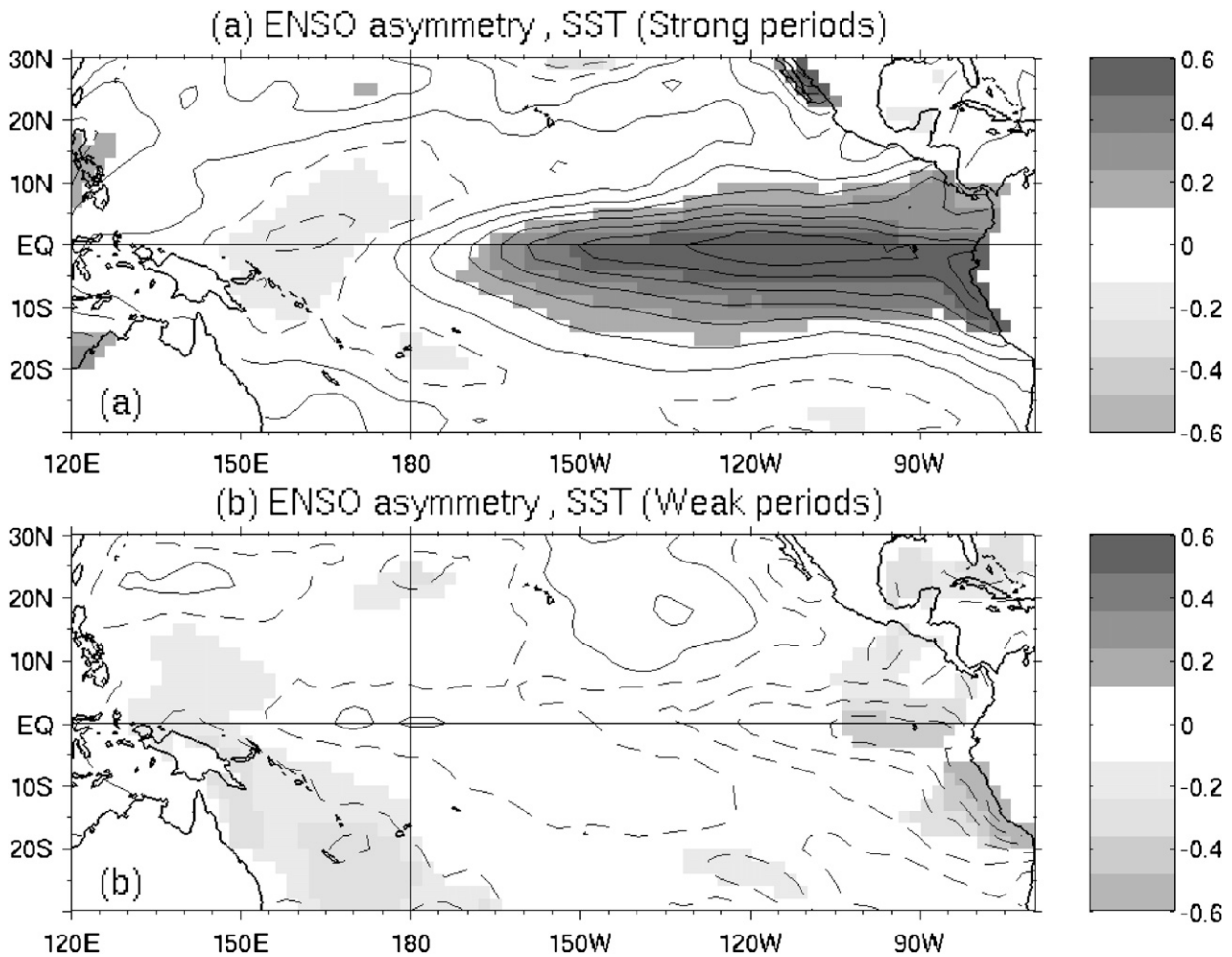
FIG. 6. The asymmetric (El Niño + La Niña) structures of extended winter SST anomalies for the (a) enhanced and (b) weakened ENSO intensity periods. CI is 0.1°C, and shading indicates the 90% SL using a two-tailed *t* test.

to the understanding of the decadal modulation of ENSO.

5. ENSO residual effect on the mean state changes

In this section, we quantify the SST asymmetry between El Niño and La Niña by the sum of their SST anomaly composites. Figure 6 shows the sums of the composite for the enhanced and weakened periods of the modulation cycle separately. During the enhanced periods, the sum exhibits large positive anomalies in the far eastern tropical Pacific (around 100°W) centered slightly to the south of equator. Comparison of Fig. 6a with the two composites in Figs. 3a and 3b indicates the positive anomalies in the eastern tropical Pacific are largely a result of that El Niño warming affect on SST being larger than the La Niña cooling affect. As a result, the average over an ENSO cycle is not zero. Negative

SST anomalies are found along the equator between 130°E and the date line. This SST asymmetry pattern during the enhanced periods looks similar to the spatial distribution of "skewness" in Burgers and Stephenson (1999, their Fig. 3a). Strong warming occurs in the far eastern upwelling regions where the thermocline is already close to the surface; therefore, it is difficult to attain much cooler than warmer SST. Strong cooling occurs in the central Pacific because of cloud feedback and surface fluxes, which limit warming SST (Rodgers et al. 2004). During the weakened periods, the sum exhibits negative anomalies in the far eastern Pacific and slightly positive anomalies in the central Pacific. This pattern is nearly out of phase with the composite sum in the enhanced periods. Because the sum of El Niño and La Niña composites represents the residual effect that ENSO asymmetry may have on the mean state, the nearly reversed patterns shown in Fig. 6
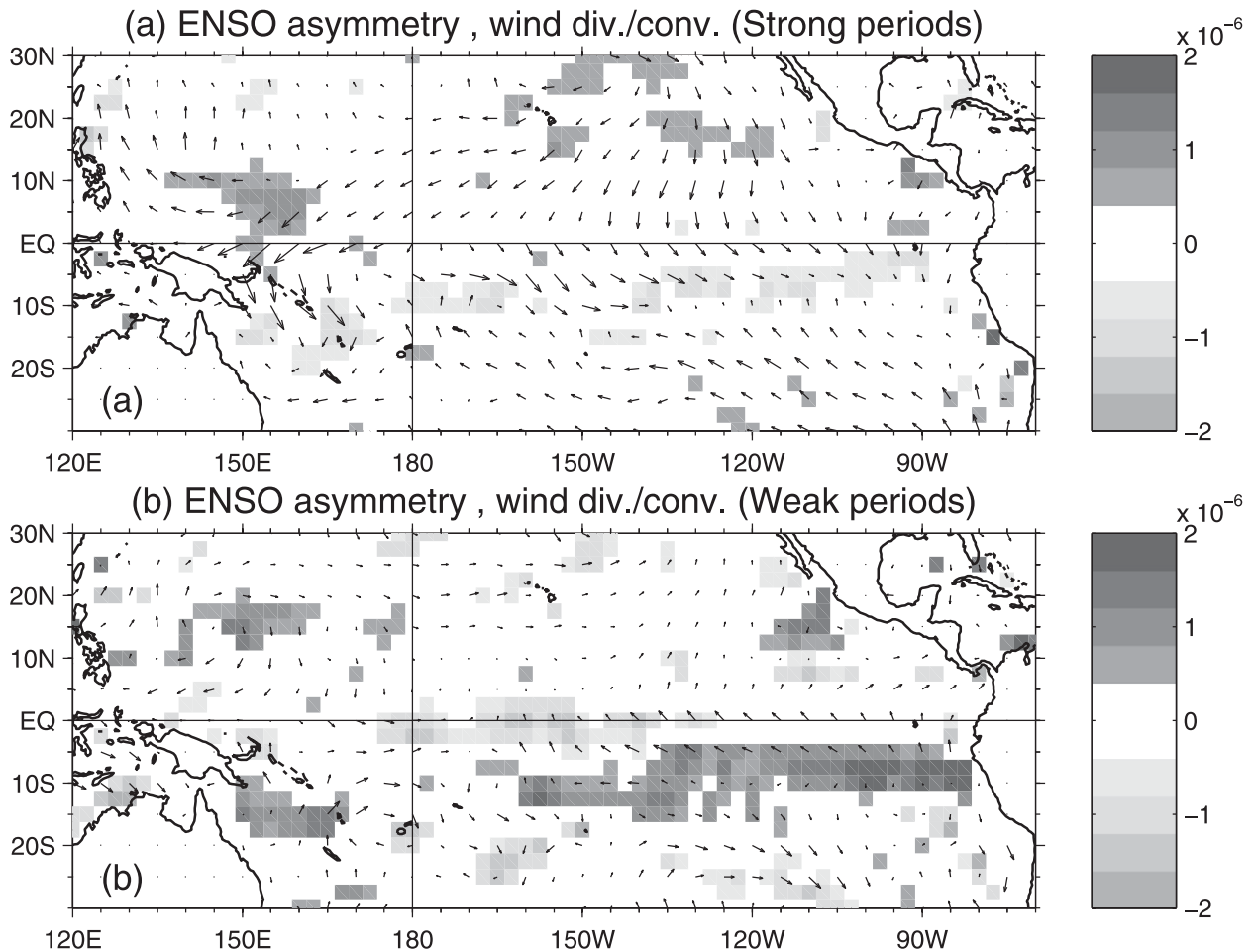
(a) ENSO asymmetry , wind div./conv. (Strong periods)

(b) ENSO asymmetry , wind div./conv. (Weak periods)

FIG. 7. As in Fig. 6, but for the surface wind vector (m s^{-1}) and divergence (dark gray) and convergence (bright gray) anomalies (m s^{-2}). Shading indicates the 90% SL using a two-tailed t test.

suggest the residual effect is reversed between the enhanced and weakened intensity periods of the 10–15-yr modulation cycle. During the enhanced intensity periods, the ENSO residual effect tends to warm up the eastern tropical Pacific but cool down the central tropical Pacific, which might lead to a decrease of the east–west SST gradient along the equator. During the weakened intensity periods, the ENSO residual effect tends to cool down the eastern tropical Pacific but warm up the central Pacific and increase the east–west SST gradient.

Figure 7 displays the sums of the composite surface wind vector and convergence/divergence anomalies for El Niño and La Niña in the enhanced and weakened intensity periods. The sums represent the ENSO residual effects on the mean surface wind. In the enhanced intensity periods (Fig. 7a), ENSO residual tends to produce northwesterly anomalies in the eastern equatorial Pacific, which is opposite of the climatological

southeasterly, representing a relaxation of the trade winds in that region. In the weakened periods (Fig. 7b), ENSO residual tends to produce southeasterly anomalies in the eastern Pacific and strengthen the climatological trade winds. Figure 7 also shows that the ENSO residuals result in anomalous surface wind convergence in the far eastern Pacific from 15°S to the equator in the enhanced intensity periods but anomalous divergence in the weakened intensity periods. The corresponding ENSO residual effects on the mean thermocline depth are shown in Fig. 8. During the enhanced intensity periods (Fig. 8a), ENSO residual tends to increase the thermocline depth in the eastern tropical Pacific but decrease the depth in the central Pacific. During the weakened intensity periods (Fig. 8b), the residual decreases the thermocline depth along the coast but increases it in the central Pacific. Significant thermocline variations in the tropical Pacific cover a region extending from around 10°S to 10°N and coincide more or less
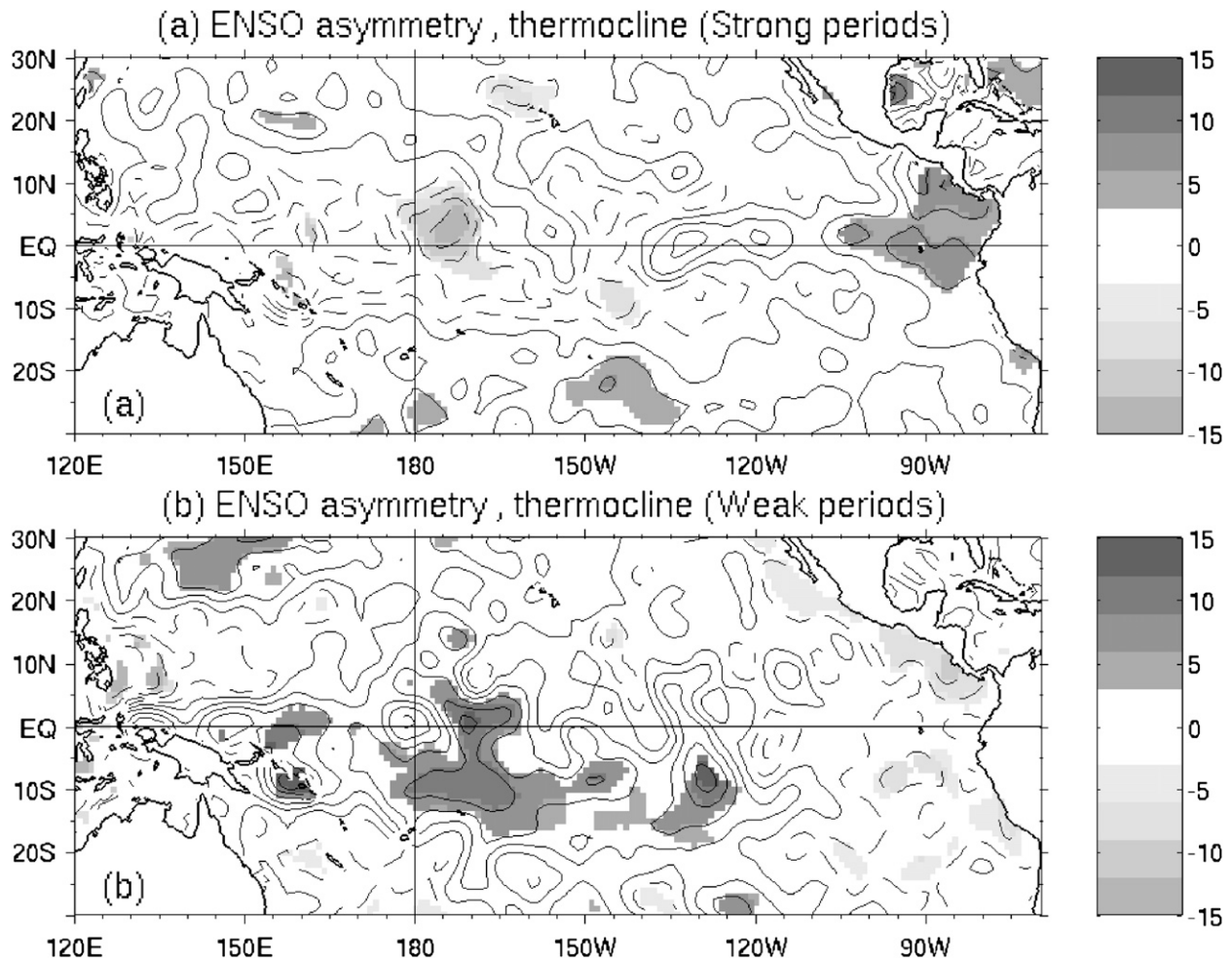
FIG. 8. As in Fig. 6, but for the 20°C isotherm depth anomalies (m). Shaded indicates the 90% significance level using a two-tailed t test. Contour interval is 3 m.

with the areas of large asymmetric patterns for the SST and surface wind shown in Figs. 6 and 7. Figures 6–8 indicate that the SST, surface wind, and thermocline depth anomalies resulting from the ENSO residual effects are dynamically consistent with each other. For example, in the enhanced intensity periods, the asymmetry between El Niño and La Niña SST anomalies tends to increase the mean SST in the eastern Pacific that in turn relaxes the mean surface trade wind in the region. The relaxed surface trade wind, together with the anomalous convergence, tends to deepen the mean thermocline and, therefore, further warms up the eastern Pacific.

To further quantify the tropical Pacific mean state changes related to the modulation cycle, we regress the bandpass-filtered ENVF against different climate variables (SST, surface wind, and thermocline depth) in Fig. 9. We have tried the analysis with both the 10-yr low-

pass-filtered and the nonfiltered anomalies for the climate variables and found little difference in the regression results. The results shown are those calculated with the nonfiltered anomalies. The regression for SST anomalies (Fig. 9a) is characterized by a nearly zonal dipole structure along the equator between the far eastern Pacific near (10°S, 90°W) and the central Pacific near (175°E). It is also noticeable that the regression center in the central Pacific is symmetric with respect to the equator, whereas the regression center in the far eastern Pacific is meridionally asymmetric and centered to the south of equator. Figure 9a indicates that in the enhanced ENSO periods, the far eastern Pacific is warmer than normal, whereas the central equatorial Pacific is cooler than normal and vice versa for the weakened periods, which is similar to the ENSO residual SST effects shown in Fig. 6. Quantitatively, when the decadal ENSO intensity increases one standard
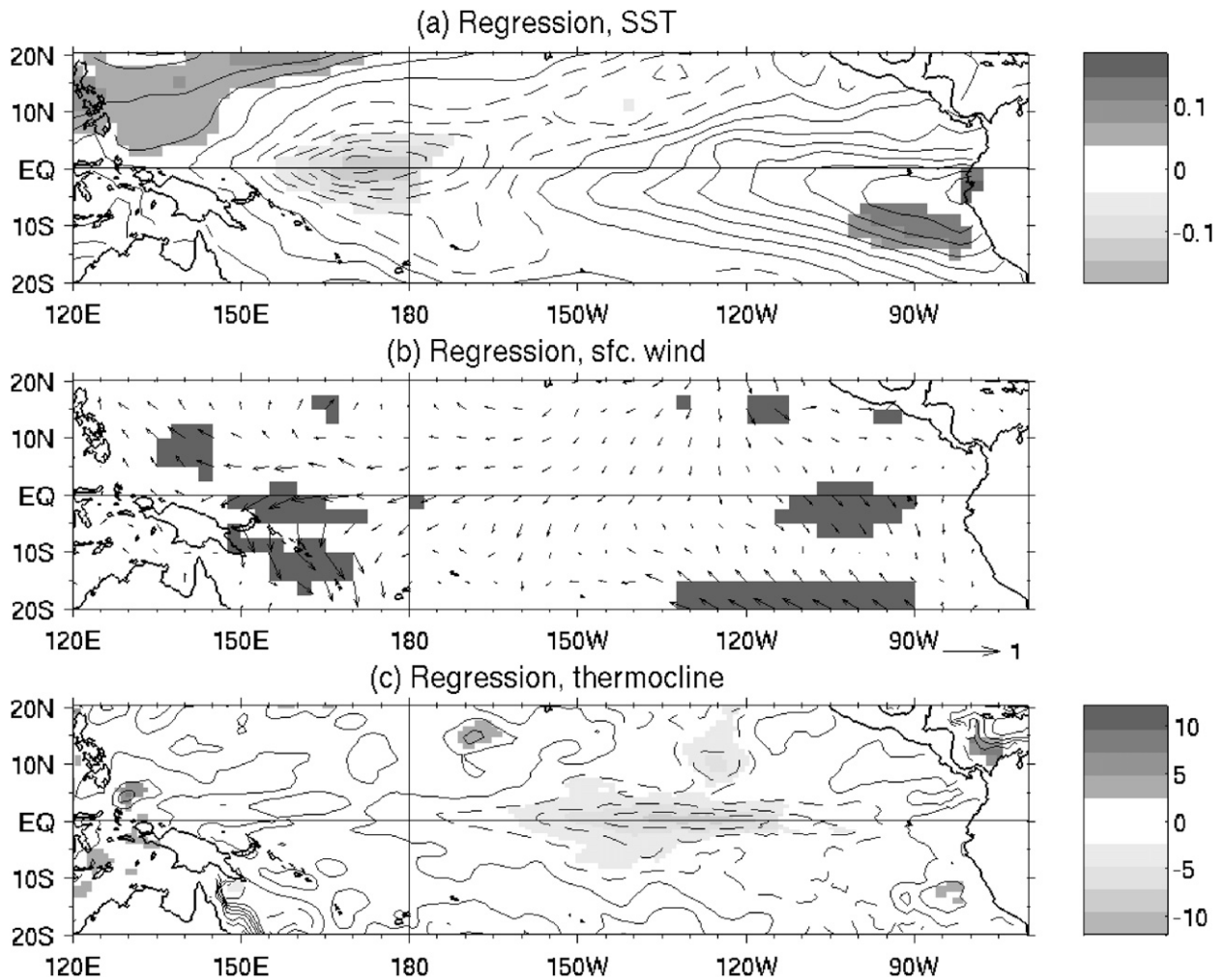
FIG. 9. (a) Linear regression between 10–20-yr bandpass-filtered ENVF (Fig. 1b) and unfiltered extended winter SST anomalies [°C (std dev)$^{-1}$ of ENVF; contour interval is 0.03°C (std dev)$^{-1}$]. (b) As in (a), but for the surface wind [m s^{-1} (std dev)$^{-1}$ of ENVF]. (c) Same as (a), but for the 20°C isotherm depth [m (std dev)$^{-1}$ of ENVF; CI is 2]. Shading indicates the 90% SL using f test.

deviation, the ENSO asymmetry warms up the eastern tropical Pacific and cools downs the central tropical Pacific by about 0.1–0.2°C.

The regression pattern for surface wind shown in Fig. 9b also is similar to the ENSO residual wind effects displayed in Fig. 7, which indicates the climatological trade winds are relaxed in the eastern tropical Pacific and strengthened in the central Pacific during the enhanced periods and vice versa for the weakened periods. Figure 9c shows the corresponding regression pattern for 20°C isotherm depth. Opposite thermocline variations appear between the far eastern tropical Pacific (centered at 10°S, 90°W) and the central equatorial Pacific (centered at 130°W). In the enhanced periods, the mean thermocline deepens in the far eastern tropical Pacific and shoals in the central Pacific. This regression pattern is, in general, consistent with the

corresponding ENSO asymmetry pattern for the thermocline depth shown in Fig. 8.

The similarities between the ENSO asymmetry residual patterns shown in Figs. 6–8 and the ENVF-regressed variation patterns shown in Fig. 9 suggest the slow variations in the Pacific mean state associated with the ENSO modulation cycle are closely related to the ENSO residual effects. So, how important are the decadal modulation of ENSO and its residual effects to the decadal mean state changes in the tropical Pacific? To answer this question, we examined the leading modes of decadal SST variability in the tropical Pacific using the empirical orthogonal function (EOF) analysis. The EOF analysis is applied to the 10–20-yr bandpass-filtered winter SST anomalies in the tropical Pacific (120°E–70°W, 30°S–30°N). The first two leading EOF modes are shown in Fig. 10, which explain 51% and
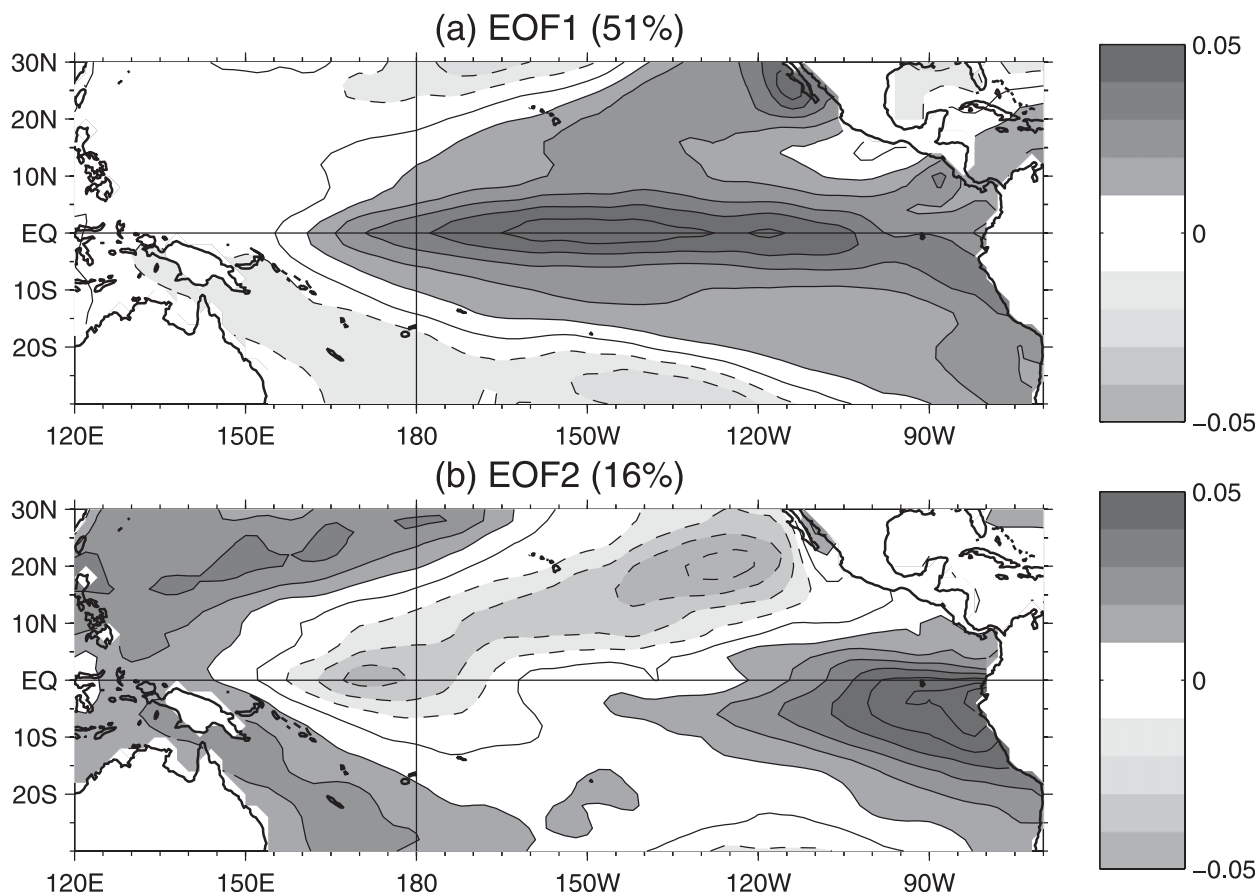
FIG. 10. The (a) first and (b) second leading EOF mode of 10–20-yr bandpass-filtered extended winter SST anomalies in the tropical Pacific (30°S–30°N, 120°E–70°W). CI is 0.01°C.

16% of the filtered SST variance, respectively. The first EOF (Fig. 10a) has a spatial structure similar to PDO or the so-called ENSO-like decadal variability (Zhang et al. 1997). This structure is characterized by a horse-shoe pattern in the eastern-to-central Pacific, flanked by opposite structures in the midlatitudes of western and central Pacific in both hemispheres. The correlation coefficient between the principal coefficient of this first EOF mode and the bandpass-filtered ENVF is small (correlation coefficient is −0.34) and does not pass the 95% significance test. This indicates that the 10–15-yr ENSO modulation cycle is not directly related to this first EOF mode. And this result is consistent with the observational study of Yeh and Kirtman (2005), who found no direct relationship between their horse-shoe EOF mode and the decadal modulation of ENSO amplitude.

The second EOF mode (Fig. 10b) exhibits a zonally out-of-phase structure between the central and eastern tropical Pacific. Also noted in this pattern is the extension of the SST anomalies from the central Pacific

to the northeast Pacific and Baja California. This EOF pattern is spatially similar to the ENVF-regressed SST pattern shown in Fig. 9a. The simultaneous correlation coefficient between the principal component of the second EOF mode and the bandpass-filtered ENVF is as large as 0.70 and is statistically significant at the 95% level. This indicates the second EOF mode reflects the mean state changes associated with the reversed ENSO residual effects within the modulation cycle. The mean state change associated with decadal ENSO modulation is an important part of the tropical Pacific decadal variability. Yeh and Kirtman (2005) even suggested the observed low-frequency ENSO modulation leads to the slow changes in the whole Pacific mean state three to four years to stress the forcing by changes in the ENSO statistics. Several CGCM studies (Timmermann 2003; Yeh and Kirtman 2004; Rodgers et al. 2004) also found the decadal modulations of their model ENSO are associated with a dipole-like tropical Pacific decadal variability similar to the second leading EOF mode we show here.
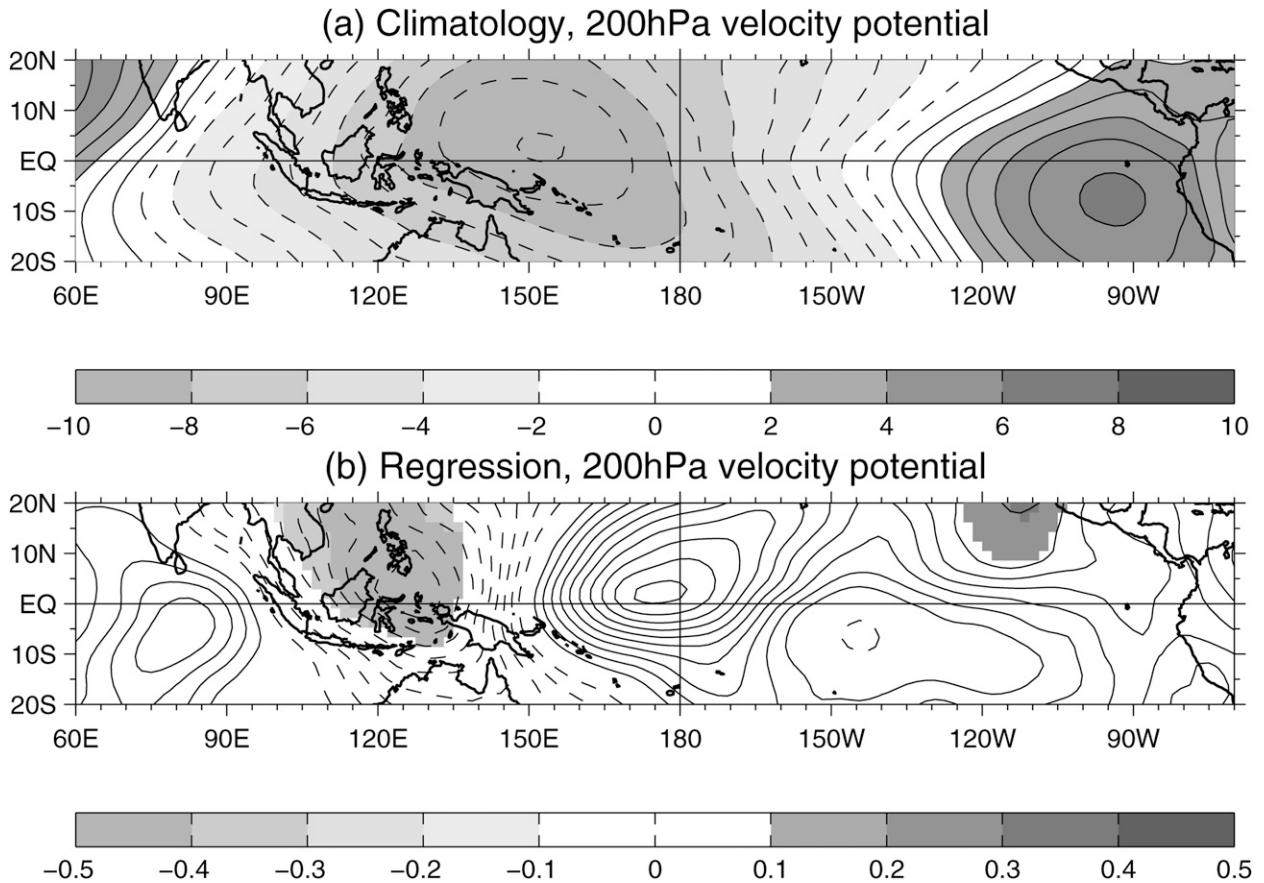
(a) Climatology, 200hPa velocity potential

(b) Regression, 200hPa velocity potential

FIG. 11. (a) Long-term mean climatology of 200-hPa velocity potential (10^6 m^2 s^{-1}) with zonal mean removed. Positive indicates sinking motion and negative indicates rising motion. (b) Linear regression between 10–20-yr bandpass-filtered ENVF and unfiltered extended winter 200-hPa velocity potential [10^6 m^2 s^{-1} (std dev)$^{-1}$ of ENVF]. Shaded indicates the 90% SL using f test.

However, there are some differences in details between the observed SST dipole pattern in our study and those model SST dipole patterns. First, the observed dipole pattern shows an out-of-phase SST anomaly pattern between the far eastern and the central tropical Pacific around the date line, whereas the one shown in Yeh and Kirtman (2004) is an out-of-phase pattern between the eastern and western tropical Pacific. Second, the dipole pattern shown in Timmermann (2003) is more confined in the equatorial Pacific, whereas the observed one has significant loadings in the off-equatorial regions, especially in the far eastern tropical Pacific. Furthermore, the observed dipole pattern is meridionally asymmetric in the far eastern Pacific but the ones reported in Timmermann (2003) and Yeh and Kirtman (2004) are exactly symmetrical to the equator there. The causes of these differences are unknown but could possibly be related to different analysis processes used or be that these CGCMs are dominated by 2-yr ENSO.

To allow the slow changes in the Pacific mean SSTs to modulate ENSO intensity, the mean SST changes have to be strong enough to affect the Pacific Walker circulation, whose location, intensity, and zonal extent exert strong influence on the strength of atmosphere–ocean coupling in the tropical Pacific (Deser and Wallace 1990). Following Tanaka et al. (2004), we measure the strength of the Walker circulation by the extended winter velocity potential at 200 hPa with its zonal mean removed. The climatology of the Pacific Walker circulation is shown in Fig. 11a, with negative values indicating rising motion with upper-troposphere divergence and positive values sinking motion with upper-troposphere convergence. The climatology is characterized by a rising branch centered over the Philippine Sea and Maritime Continent near 150°E and a sinking branch centered over the far eastern tropical Pacific and Central American continents around 10°S and 100°W.

The variations of the Walker circulation associated with the decadal modulation of ENSO intensity is examined

in Fig. 11b by regressing the bandpass-filtered ENVF against the unfiltered 200-hPa velocity potential anomalies. It shows the locations of both rising and sinking branches of the Walker circulation associated with the slowly varying ENSO intensity cycle. The regression pattern exhibits a seesaw anomalous structure to the west and east of the climatological rising center of the Walker circulation. The rising branch in the western Pacific moves westward to 120°E during the enhanced ENSO intensity periods and eastward to the date line during the weakened periods. The sinking branch in the eastern Pacific also migrates during the ENSO modulation cycle. Compared with the climatology, the sinking branch shifts northwestward during the enhanced periods. It appears that the Pacific Walker circulation shifts westward during the enhanced periods and eastward during the weakened periods. It is noticed that this pattern is dynamically consistent with the surface wind pattern in Fig. 9b in which easterlies in western equatorial Pacific (e.g., over Indonesia) are strengthened (relaxed), corresponding to the westward-shifted (eastward shifted) Walker circulation during the enhanced (weakened) ENSO intensity periods.

6. Conclusions and discussion

As one of the most pronounced interannual climate signal in tropical Pacific, ENSO also shows decadal variations, which have captured more and more attention in the climate research community. By analyzing historical and paleo-proxy climate datasets, we investigated the decadal modulation of ENSO intensity and the ENSO residual effects on the Pacific mean state. We find the ENSO intensity exhibits a prominent 10–15-yr modulation cycle and this verifies the previous studies (e.g., Gu and Philander 1995; Knutson et al. 1997; Kirtman and Schopf 1998; Torrence and Webster 1999). The modulation cycle is characterized by evident spatial asymmetry between El Niño and La Niña events, which allows the ENSO cycle to leave a nonzero residual effect onto the mean state changes in the tropical Pacific. And the spatial asymmetry is reversed between the enhanced and weakened intensity periods of the modulation cycle, which implies opposite residual effects were produced by ENSO on the Pacific mean state during different periods of the modulation cycle. The mean state changes associated with the modulation cycle appears as the second leading EOF mode of the decadal SST variations in the tropical Pacific. It suggests the decadal ENSO variability is an important source of tropical Pacific decadal variability. This substantiates the previous studies (e.g., Rodgers et al. 2004; Yeh and Kirtman 2004, 2005; and Schopf
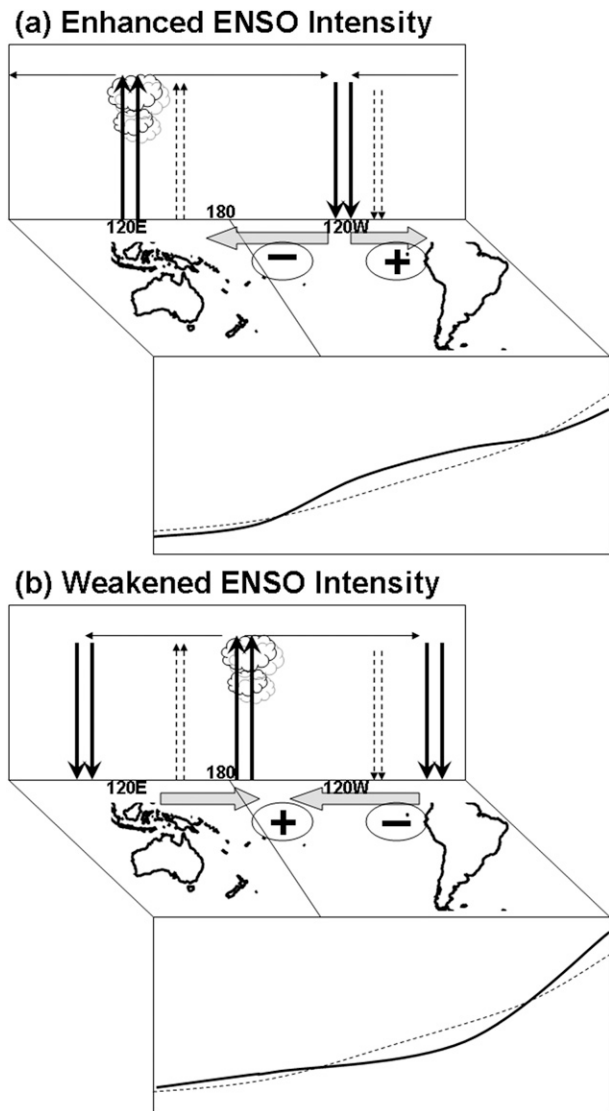

FIG. 12. Schematic diagram showing the oceanic and atmospheric variations in the tropical Pacific caused by El Niño–La Niña asymmetry forcing during the (a) enhanced and (b) weakened ENSO intensity periods. Dashed lines show the climatology.

and Burgman 2006) on the forces of ENSO statistics on the Pacific mean state.

Figure 12 is sketched to summarize the major features in the changes of Pacific mean state within the modulation cycle. In the enhanced intensity periods of the cycle (Fig. 12a), the El Niño–La Niña asymmetry results in a westward shift of the Walker circulation compared to its climatology, which strengthens the trade winds and favors cooling in the central tropical Pacific but relaxes the trade winds and favors warming in the eastern tropical Pacific. Accompanied with the circulation shift is the flattened thermocline along the

equator, with a deepening thermocline in the far eastern and a shoaling thermocline in the central Pacific. The resulted mean state changes should weaken the atmosphere–ocean coupling in the Pacific and shift the Pacific coupled system into the weakened ENSO intensity periods. In this Pacific mean state, the already deeper-than-normal thermocline in the eastern tropical Pacific may make local SSTs more sensitive to upwelling than to downwelling. As a result, it favors La Niña but prohibits El Niño from occurring in the eastern tropical Pacific. This may be one possible reason why the El Niño–La Niña asymmetry reverses during the weakened intensity periods. Figure 12b shows that in these weakened ENSO intensity periods, the mean state changes associated with the ENSO residual effect are characterized by a gradual cooling in the far eastern Pacific and a warming in the central-western Pacific. Associated with the SST variations are strengthened and relaxed trade winds in these two regions, respectively, via the eastward migration of the Walker circulation from its climatology locations. The changes lead to the rebuilding of the zonal SST gradient along the equator and concurrent deepening and shoaling of the thermocline in the central and eastern tropical Pacific, respectively. As a result, the ocean–atmosphere coupling is enhanced in the Pacific by the ENSO residual effect and the Pacific mean state is gradually pushed back to the enhanced ENSO intensity periods. In the enhanced periods, the shallower-than-normal thermocline in the eastern tropical Pacific may be more sensitive to downwelling than upwelling. Therefore, it favors El Niño to happen in the eastern Pacific but prohibits La Niña there.

Our studies indicate that a two-way interaction mechanism between the ENSO asymmetry and tropical Pacific mean state may operate in the tropical Pacific to support a 10–15-yr modulation cycle of ENSO intensity. And our results substantiate the importance of ENSO's regulatory effects, and they are in agreement with the recent numerical modeling studies (e.g., Sun and Zhang 2006 and Sun 2007) that suggested ENSO can have regulatory effects on the tropical Pacific mean climate. Our results further suggest that better understanding of the ENSO asymmetry and its residual influences on the Pacific mean state is important to the study of the decadal ENSO variations. The mechanism we hypothesized here relies on the reversible ENSO residual effects on the Pacific mean state to provide the needed restoring force to sustain the modulation cycle. A few issues have yet to be addressed to examine this ENSO–Pacific mean state interaction mechanism. The ENSO asymmetry residual effect may have different interpretations in other studies. For example, as elaborated by Schopf and Burgman (2006), they presented a kinematic effect of oscillating a nonlinear temperature profile similar to that seen in the equatorial Pacific to account for the long-term mean state changes as ENSO intensity changes. Though the residual effects of ENSO cycle on the mean state are likely, they should not have an influence on the stability of the underlying system or the future evolution of the system. Therefore, it has yet to be demonstrated that the ENSO residual effect does constitute as a forcing to the Pacific mean state, which in turn affects the ENSO properties. Also, the interaction mechanism we postulated here invokes a linearity assumption in which the Pacific state is assumed to fluctuate around a stationary basic state to determine the properties of ENSO. It has yet to be determined how useful this linear view can be used to explain nonlinear ENSO behaviors. Another issue that has yet to be understood is how the 10–15-yr modulation time scale is determined. Further examinations and verifications of the ENSO–Pacific mean state interaction hypothesis proposed here are needed.

REFERENCES

Alexander, M. A., I. Bladé, M. Newman, J. R. Lanzante, N. C. Lau, and J. D. Scott, 2002: The atmospheric bridge: The influence of ENSO teleconnections on air–sea interaction over the global oceans. *J. Climate,* **15,** 2205–2231.

An, S. I., and B. Wang, 2000: Interdecadal change of the structure of the ENSO mode and its impact on the ENSO frequency. *J. Climate,* **13,** 2044–2055.

——, and F.-F. Jin, 2004: Nonlinearity and asymmetry of ENSO. *J. Climate,* **17,** 2399–2412.

Barnett, T. P., D. W. Pierce, M. Latif, D. Dommenget, and R. Saravanan, 1999: Interdecadal interactions between the tropics and midlatitudes in the Pacific basin. *Geophys. Res. Lett.,* **26,** 615–618.

Battisti, D. S., and A. C. Hirst, 1989: Interannual variability in the tropical atmosphere–ocean system: Influences of the basic state, ocean geometry, and nonlinearity. *J. Atmos. Sci.,* **46,** 1687–1712.

Burgers, G., and D. B. Stephenson, 1999: The "normality" of El Niño. *Geophys. Res. Lett.,* **26,** 1027–1030.

Carton, J. A., G. Chepurin, X. H. Cao, and B. Giese, 2000: A simple ocean data assimilation analysis of the global upper ocean 1950–95. Part I: Methodology. *J. Phys. Oceanogr.,* **30,** 294–309.

Deser, C., and J. M. Wallace, 1990: Large-scale atmospheric circulation features of warm and cold episodes in the tropical Pacific. *J. Climate,* **3,** 1254–1281.

——, A. S. Phillips, and J. W. Hurrell, 2004: Pacific interdecadal climate variability: Linkages between the tropics and the North Pacific during boreal winter since 1900. *J. Climate,* **17,** 3109–3124.

Dong, B.-W., 2005: Asymmetry between El Niño and La Niña in a global coupled GCM with an eddy-permitting ocean resolution. *J. Climate,* **18,** 3084–3098.

Eckert, C., and M. Latif, 1997: Predictability of a stochastically forced hybrid coupled model of El Niño. *J. Climate,* **10,** 1488–1504.

Fedorov, A. V., and S. G. Philander, 2000: Is El Niño changing? *Science,* **288,** 1997–2002.

Gu, D., and S. G. H. Philander, 1995: Secular changes of annual and interannual variability in the tropics during the past century. *J. Climate,* **8,** 864–876.

——, and ——, 1997: Interdecadal climate fluctuations that depend on exchanges between the tropics and extratropics. *Science,* **275,** 805–807.

Hoerling, M. P., A. Kumar, and M. Zhong, 1997: El Niño, La Niña, and the nonlinearity of their teleconnections. *J. Climate,* **10,** 1769–1786.

Jin, F.-F., and J. D. Neelin, 1993a: Modes of interannual tropical ocean–atmosphere interaction—A unified view. Part I: Numerical results. *J. Atmos. Sci.,* **50,** 3477–3503.

——, and ——, 1993b: Modes of interannual tropical ocean–atmosphere interaction—A unified view. Part III: Analytical results in fully coupled cases. *J. Atmos. Sci.,* **50,** 3523–3540.

Kalnay, E., and Coauthors, 1996: The NCEP/NCAR 40-Year Reanalysis Project. *Bull. Amer. Meteor. Soc.,* **77,** 437–471.

Kao, H.-Y., and J.-Y. Yu, 2009: Contrasting eastern-Pacific and central-Pacific types of ENSO. *J. Climate,* **22,** 615–632.

Kirtman, B. P., and P. S. Schopf, 1998: Decadal variability in ENSO predictability and prediction. *J. Climate,* **11,** 2804–2822.

Knutson, T. R., S. Manabe, and D. Gu, 1997: Simulated ENSO in a global coupled ocean–atmosphere model: Multidecadal amplitude modulation and CO_2 sensitivity. *J. Climate,* **10,** 131–161.

Latif, M., A. Sterl, E. Majer-Reimer, and W. M. Junge, 1993: Climate variability in a coupled GCM. Part I: The tropical Pacific. *J. Climate,* **6,** 5–21.

Levitus, S., J. Antonov, and T. Boyer, 2005: Warming of the world ocean, 1955–2003. *Geophys. Res. Lett.,* **32,** L02604, doi:10.1029/2004GL021592.

Mann, M. E., E. Gille, R. S. Bradley, M. K. Hughes, J. Overpeck, F. T. Keimig, and W. Gross, 2000: Global temperature patterns in past centuries: An interactive presentation. *Earth Interactions* **4.** [Available online at http://EarthInteractions.org.]

Mantua, N. J., S. R. Hare, Y. Zhang, J. M. Wallace, and R. C. Francis, 1997: A Pacific interdecadal climate oscillation with impacts on salmon production. *Bull. Amer. Meteor. Soc.,* **78,** 1069–1079.

Meehl, G. A., P. Gent, J. M. Arblaster, B. Otto-Bliesner, E. Brady, and A. Craig, 2001: Factors that affect amplitude of El Niño in global coupled climate models. *Climate Dyn.,* **17,** 515–526.

Monahan, A. H., 2001: Nonlinear principal component analysis: Tropical Indo–Pacific sea surface temperature and sea level pressure. *J. Climate,* **14,** 219–233.

Nakamura, H., and J. M. Wallace, 1990: Observed changes in baroclinic wave activity during the life cycles of low-frequency circulation anomalies. *J. Atmos. Sci.,* **47,** 1100–1116.

Neelin, J. D., 1991: The slow sea surface temperature mode and the fast-wave limit: Analytic theory for tropical interannual oscillations and experiments in a hybrid coupled model. *J. Atmos. Sci.,* **48,** 584–606.

——, and F.-F. Jin, 1993: Modes of interannual tropical ocean–atmosphere interaction—A unified view. Part II: Analytical results in the weak-coupling limit. *J. Atmos. Sci.,* **50,** 3504–3522.

Newman, M., 2007: Interannual to decadal predictability of tropical and North Pacific sea surface temperatures. *J. Climate,* **20,** 2333–2356.

——, G. P. Compo, and M. A. Alexander, 2003: ENSO-forced variability of the Pacific decadal oscillation. *J. Climate,* **16,** 3853–3857.

Parks, T. W., and C. S. Burrus, 1987: Design of linear-phase finite impulse-response. *Digital Filter Design,* John Wiley & Sons, 33–110.

Penland, C., and P. D. Sardeshmukh, 1995: The optimal growth of tropical sea surface temperature anomalies. *J. Climate,* **8,** 1999–2024.

Pierce, D. W., T. P. Barnett, and M. Latif, 2000: Connections between the Pacific Ocean tropics and midlatitudes on decadal timescales. *J. Climate,* **13,** 1173–1194.

Power, S., T. Casey, C. Folland, A. Colman, and V. Mehta, 1999: Inter-decadal modulation of the impact of ENSO on Australia. *Climate Dyn.,* **15,** 319–324.

Rasmusson, E. M., and T. H. Carpenter, 1982: Variations in tropical sea surface temperature and surface wind fields associated with the Southern Oscillation/El Niño. *Mon. Wea. Rev.,* **110,** 354–384.

Rayner, N. A., D. E. Parker, E. B. Horton, C. K. Folland, L. V. Alexander, D. P. Rowell, E. C. Kent, and A. Kaplan, 2003: Global analyses of sea surface temperature, sea ice, and night marine air temperature since the late nineteenth century. *J. Geophys. Res.,* **108,** 4407, doi:10.1029/2002JD002670.

Rodgers, K. B., P. Friederichs, and M. Latif, 2004: Tropical Pacific decadal variability and its relation to decadal modulations of ENSO. *J. Climate,* **17,** 3761–3774.

Schopf, P. S., and R. J. Burgman, 2006: A simple mechanism for ENSO residuals and asymmetry. *J. Climate,* **19,** 3167–3179.

Smith, T. M., and R. W. Reynolds, 2003: Extended reconstruction of global sea surface temperatures based on COADS data (1854–1997). *J. Climate,* **16,** 1495–1510.

——, and ——, 2004: Improved extended reconstruction of SST (1854–1997). *J. Climate,* **17,** 2466–2477.

Suarez, M. J., and P. S. Schopf, 1988: A delayed action oscillator for ENSO. *J. Atmos. Sci.,* **45,** 3283–3287.

Sun, D.-Z., 2007: The role of ENSO in regulating its background state. *Nonlinear Dynamics in Geosciences,* Springer, 604 pp.

——, and T. Zhang, 2006: A regulatory effect of ENSO on the time-mean thermal stratification of the equatorial upper ocean. *Geophys. Res. Lett.,* **33,** L07710, doi:10.1029/2005GL025296.

Tanaka, H. L., N. Ishizaki, and A. Kitoh, 2004: Trend and interannual variability of Walker, monsoon and Hadley circulations defined by velocity potential in the upper troposphere. *Tellus,* **56A,** 250–269.

Timmermann, A., 2003: Decadal ENSO amplitude modulations: A nonlinear paradigm. *Global Planet. Change,* **37,** 135–156.

——, and F.-F. Jin, 2002: A nonlinear mechanism for decadal El Niño amplitude changes. *Geophys. Res. Lett.,* **29,** 1003, doi:10.1029/2001GL013369.

Torrence, C., and P. J. Webster, 1999: Interdecadal changes in the ENSO–monsoon system. *J. Climate,* **12,** 2679–2690.

Troup, A. J., 1965: The "southern oscillation." *Quart. J. Roy. Meteor. Soc.,* **91,** 490–506.

Wang, B., and Y. Wang, 1996: Temporal structure of the Southern Oscillation as revealed by waveform and wavelet analysis. *J. Climate,* **9,** 1586–1598.

Wang, C. Z., and R. H. Weisberg, 1998: Climate variability of the coupled tropical–extratropical ocean–atmosphere system. *Geophys. Res. Lett.,* **25,** 3979–3982.

Wilks, D.S., 1995: *Statistical Methods in the Atmospheric Sciences.* International Geophysics Series, Vol. 59, Academic Press, 464 pp.

Yeh, S.-W., and B. P. Kirtman, 2004: Tropical Pacific decadal variability and ENSO amplitude modulation in a CGCM. *J. Geophys. Res.,* **109,** C11009, doi:10.1029/2004JC002442.

——, and ——, 2005: Pacific decadal variability and decadal ENSO amplitude modulation. *Geophys. Res. Lett.,* **32,** L05703, doi:10.1029/2004GL021731.

Zebiak, S. E., and M. A. Cane, 1987: A model for El Niño–Southern Oscillation. *Mon. Wea. Rev.,* **115,** 2262–2278.

Zhang, X. B., J. Sheng, and A. Shabbar, 1998: Modes of interannual and interdecadal variability of Pacific SST. *J. Climate,* **11,** 2556–2569.

Zhang, Y., J. M. Wallace, and D. S. Battisti, 1997: ENSO-like interdecadal variability: 1900–93. *J. Climate,* **10,** 1004–1020.